

Modeling Disordered Quantum-Systems with Dynamical Networks

Rochus Klesse¹ and Marcus Metzler²

Institut für Theoretische Physik, Universität zu Köln, D-50937 Köln, Germany

(February 1, 2008)

It is the purpose of the present article to show that so-called network models, originally designed to describe static properties of disordered electronic systems, can be easily generalized to quantum-*dynamical* models, which then allow for an investigation of dynamical and spectral aspects. This concept is exemplified by the Chalker-Coddington model for the Quantum Hall effect and a three-dimensional generalization of it. We simulate phase coherent diffusion of wave packets and consider spatial and spectral correlations of network eigenstates as well as the distribution of (quasi-)energy levels. Apart from that it is demonstrated how network models can be used to determine two-point conductances. Our numerical calculations for the three-dimensional model at the Metal-Insulator transition point delivers among others an anomalous diffusion exponent of $\eta = 3 - D_2 = 1.7 \pm 0.1$. The methods presented here in detail have been used partially in earlier work.

I. INTRODUCTION

Models formulated in scattering theoretical terms have been proven to be convenient for the investigation of quantum particle- or classical wave-propagation in disordered media. Examples related to Anderson localization [1] are the scattering model of a one-dimensional (1D) disordered conductor used by Anderson et al. [2], it's three-dimensional (3D) version introduced by Shapiro [3], and the Chalker-Coddington network of the Quantum Hall transition [4]. Numerous generalizations and variations of these models have been used in order to study various topics in different fields [5–10].

The common concept in these approaches is the scattering theoretical formulation of the problem. This leads to models which can be described as networks consisting of an array of local scattering centers, linked together by 1D channels [3]. Usually, the *static* properties of these models are investigated, like probabilities for scattering through the network or correlations of stationary scattering states.

It is the purpose of the present article to show that in general these models can be easily extended to *dynamical* network models, which then allow to study dynamical as well as spectral aspects of the respective problem under consideration. In particular, we consider dynamical versions of the Chalker-Coddington model and of a 3D generalization of it [10]. Within these models we investigate numerically phase coherent diffusion of wave-packets, whereby special attention is paid to anomalous diffusion near the localization-delocalization transition point. It is demonstrated how spectral information can be extracted from these models, like (quasi-)energy spectra or the local density of states. Moreover, we present an example within the framework of a network model for determining conductances of an integer quantum Hall system contacted by point-contacts.

A network model is mathematically formulated by an explicitly defined unitary matrix, the network operator U , that determines the scattering processes between internal network channels. By definition, in the dynamical model this operator U will describe the evolution of network-states Ψ over a microscopic time interval τ , $\Psi \xrightarrow{\tau} U\Psi$. By this, a discrete time evolution is given: $\Psi(k\tau) = U^k\Psi(0)$, where $k = 0, 1, 2, \dots$. Further, network eigenstates Φ_n are defined as eigenvectors of U . The phases $\omega_n \in [0, 2\pi[$ of the unimodular eigenvalues $\exp(i\omega_n)$ will be interpreted as quasi-energy levels.

The main part of this work consists of numerical simulations within the two aforementioned models in order to demonstrate that the concept of dynamical networks is self-consistent and, above all, that it delivers results consistent with previous results and general theory of disordered systems. These simulations also clearly show that network models are convenient for numerical purposes. They allow e.g. to calculate efficiently the (fully phase coherent) time evolution of wave-packets diffusing in comparably large systems. Furthermore, the particle energy (to be distinguished from the network specific quasi-energy), becomes simply a parameter of the model. Due to this it is possible to focus at specific and sharply defined energy regimes, which will turn out to be advantageous when investigating critical level statistics.

Our approach is related to that of Edrei et al. [6], where a network model has been used for calculating wave propagation through random media. Actually, the definition of network states and operator used here are, in principle, identical to those in [6]. However, their work concentrated on stationary states of networks with open boundaries in order to determine transmission coefficients. In contrast to that, here we study the time evolution explicitly and consider in particular closed systems. The latter offers the opportunity to define and to investigate correlations of network eigenstates and quasi-energy levels.

Viewed as a time evolution operator, the network operator is also related to so called quantum maps or Floquet operators, which attracted recently considerable attention in quantum chaology [11]. It seems to be that dynamical networks and quantum maps are identical concepts, applied in different physical contexts: the former to diffusive, the latter to chaotic systems. However, the precise relation between these two classes of systems is not entirely clear to us yet and deserves further investigation in the future.

The concepts presented here have been applied partially in previous work, e.g. for determining critical eigenstates [9], local density of states [12], critical level statistics [13–15] and quantum diffusion [16]. Here we explain in more detail the numerical methods used therein. However, also the reader not familiar with network models might find this paper worth reading, since it deals with current topics in the field of critical disordered systems, like the multifractality of the local density of states, critical diffusion or energy level correlations.

The article is organized as follows: We start with a definition of dynamical network models, which tries to be a compromise between exactness and generality on the one hand and the amount of formal effort on the other. Next is the introduction of the two specific models mentioned above, within which several numerical simulations will be performed. Beginning with the simulation of diffusing wave packets we come to the calculation of the local spectral density. After that we turn to the distribution of network quasi-energy levels. The next section is concerned with correlations in the local density of critical network states, followed by a section in which the network model is used for the calculation of two-point conductances. We conclude with a summary and general remarks.

II. GENERAL DEFINITIONS

Consider a d -dimensional array of scattering centers, where each of them has n outgoing and incoming channels. Let them be labeled by a lattice index j and characterized by $n \times n$ unitary matrices S_j . Then, connecting in a certain manner outgoing with incoming channels of neighboring scatterers, one ends up with a network (Fig. 1). We denote its scattering centers as *nodes* and internal channels as *links*, labeled by another index l .

A network is closed when all channels start from and end in network nodes, otherwise it is open. In the latter case some channels start from or end somewhere outside the network, forming input (I_m) and output channels (O_l) of the network. Thereby, the number N_c of input channels always equals the number of output channels. Such an open network can be viewed as a scatterer with a complex internal structure and the transmission through it can be described by an N_c dimensional matrix \mathcal{S} , which maps the input amplitudes in I_m to the output channels

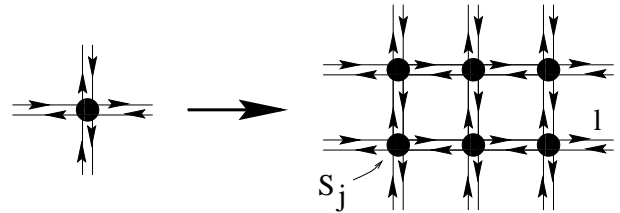


FIG. 1. The basic module of a network are elementary scatterers of the same type.

O_l . Both types of networks are illustrated by examples shown in Fig. 2.

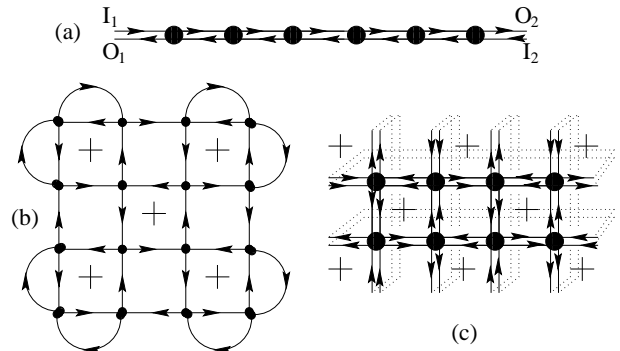


FIG. 2. Several networks of various dimensions and channel numbers n : (a) a 1D network with $n = 2$ modeling a 1D chain of scatterers. (b) the two dimensional Chalker-Coddington network for the integer quantum Hall Effect, $n = 2$. (c) the same as (b), but with spin degree of freedom, thus here $n = 4$. The network (a) is open, (b) shows an example of a closed network with reflective boundaries whereas the closed network (c) has periodic boundary conditions.

The open network (a) would be for example appropriate for the study of transmission or conductance [6], whereas the closed networks (b) and (c) could be used e.g. for determining eigenstates, as we will see in the following sections.

One can choose reflecting or periodic boundaries for the network. Reflecting boundaries are realized by bending the outgoing channels of one side to neighbored incoming ones of the same side, periodic boundaries by linking the outgoing channels to the incoming ones of the opposite side (see Fig. 2, (b) and (c)).

A network state can be introduced as the set of complex amplitudes ψ_l for all links $l = 1, \dots, N$, $\Psi = \{\psi_l\}$. Per definition, the network states form a vector space, spanned e.g. by the orthonormal unit states $\mathbf{e}_{l'} = \{\delta_{l'l}\}$. The scalar product is given by $\langle \Phi, \Psi \rangle = \sum \phi_l^* \psi_l$. When the states are interpreted as wave functions of a particle, the squared amplitude $|\psi_l|^2 = |\langle \mathbf{e}_l, \Psi \rangle|^2$ of a normalized state denotes the probability to find the particle on link l .

In physically realized networks only those states Ψ are

feasible, which have link amplitudes ψ_l obeying the scattering condition at every node of the network. This means that for every outgoing link l of a node j with a scattering matrix $S_j = \{t_{lm}^j\}$ the equation

$$\psi_l = \sum_{m:l} t_{lm}^j \psi_m \quad (1)$$

has to be fulfilled, whereby m runs over the n incoming links of that scatterer j from which link l exits (indicated by the symbol $m:l$). Stationary or steady states of the network are states satisfying this condition at each node.

The right hand side of the stationarity condition Eq. (1) can be read as the action of an operator U on the state $\Psi = \{\psi_l\}$,

$$(U\Psi)_l = \sum_{k=1}^N U_{lk} \psi_k \equiv \sum_{m:l} t_{lm}^j \psi_m.$$

Notice that the second sum contains only n summands, and not N (number of all links in the network) as in the first. This implies that only n of the N coefficients $\{U_{lk}\}_{k=1,\dots,N}$ are non-vanishing (i.e. U_{lk} is a *sparse* N -dimensional matrix). For closed networks, this operator U is unitary due to the unitarity of the local scattering matrices S_j . Obviously, the stationarity condition for a state Ψ can then be written as

$$U\Psi = \Psi. \quad (2)$$

For open networks U is no longer unitary, because in that case the probability density conservation is violated by the leakage at the outgoing channels. In this case U can still be used to formulate the stationarity condition, however, additional care has to be taken of the open input and output channels. We will discuss this in detail for one example in Sec. VII.

It is instructive to consider the action of U on a basic state \mathbf{e}_l ,

$$U\mathbf{e}_l = \sum_{m:l} t_{ml}^j \mathbf{e}_m, \quad (3)$$

where the sum runs over all outgoing links m of scatterer j in which l enters (denoted by $l:m$). Operator U simply maps the incoming amplitude to the outgoing links of the scatterer according to the transmission coefficients t_{lm}^j (Fig. 3). A corresponding physical process can be thought of as the scattering of an incident wave-packet at a node into the outgoing channels after a characteristic time τ . Therefore it is suggestive to consider the action of U on an arbitrary network state Ψ as its time evolution over a certain microscopic time interval τ ,

$$\Psi(t_0 + \tau) \equiv U\Psi(t_0). \quad (4)$$

By this, a dynamic for the network is defined by a step-wise time evolution

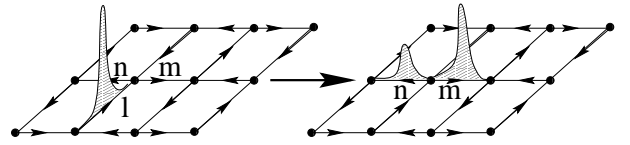


FIG. 3. The action of U on a basic state \mathbf{e}_l . It maps the incoming amplitude into the outgoing channels m, n according to the transmission coefficients t_{ml}, t_{nl} . The corresponding physical process can be thought of as the scattering of an incident wave packet into the outgoing channels after a characteristic time τ .

$$\Psi(t_0 + k\tau) = U^k \Psi(t_0) \quad (5)$$

for an integer number of time steps $k = 0, \pm 1, \pm 2, \dots$ (In the following we often set $\tau \equiv 1$ and then write $\Psi(t) = U^t \Psi(0)$.) Apparently, stationary states remain unchanged by these dynamics, as it should be.

According to these dynamics, for closed networks a real spectrum $\{\omega_n\}$ is given by the phases ω_n of the complex eigenvalues of U ,

$$U\Phi_n = e^{i\omega_n} \Phi_n. \quad (6)$$

In order to avoid ambiguity we restrict the phases or quasi-energies to $[0, 2\pi[$. With respect to the dynamics (5) the corresponding eigenvectors Φ_n oscillate with frequencies ω_n ,

$$\Phi_n(t) = U^t \Phi_n(0) = e^{i\omega_n t} \Phi_n(0). \quad (7)$$

Additionally, we define a local density of network states (LDOS) by

$$\rho_l(\omega) = \sum_n |\phi_{n,l}|^2 \delta(\omega - \omega_n). \quad (8)$$

III. SPECIAL NETWORK MODELS

After we have introduced network models in general, let us now consider two special models in more detail: the two-dimensional (2D) network introduced by Chalker and Coddington [4] to describe Quantum-Hall systems and a 3D network very similar to the model proposed by Chalker and Dohmen to describe multi-layer systems [10]. Originally, both models are purely static, but they can be easily extended to dynamical models by providing them with the discrete time evolution (5), as we will do here.

The Chalker-Coddington network is designed in the style of the networks introduced by Anderson et al. [2] and Shapiro [3] in the early 1980s, where a scattering formalism is used to describe Anderson localization. It provides a semi-classical description of a 2D electron in a strong perpendicular magnetic field B and a potential

V . The random potential V is assumed to be smooth with a correlation length a large compared to the magnetic length l_c [17–22]. Classically, the electron executes a fast cyclotron motion on a circle of radius l_c , the center of which drifts slowly along contours $V(r) = \text{const.}$. For $l_c \ll a$ it is justified to separate cyclotron and drift motion. Quantizing the first yields the Landau energies $E_n = \hbar\omega(n + \frac{1}{2})$. The drift of the center coordinate can be treated semi-classically by a WKB- or stationary-phase-approximation [17,18,20], leading to the following picture: The probability density of an eigenstate at energy E in the n th Landau band is concentrated along contours $V(c_l) \equiv E - E_n$ of the disorder potential. In local coordinates u, v parallel (u) and transverse (v) to a contour l the wave function $\Psi_E(r)$ can be well approximated by

$$\Psi_E(u, v) = \psi_l \frac{1}{\sqrt{v_d(u)}} \varphi_n(v/l_c) e^{i\phi(u, v)}, \quad (9)$$

where $\varphi_n(x)$ denotes the n th Hermite polynomial and $\phi(u, v)$ a gauge dependent phase. Because of the normalization by the local drift velocity $v_d(u)$, the squared modulus of the complex coefficient ψ_l gives the net current transported by the state along the contour l in direction of the drift motion. The approximation is valid everywhere where the contour line is well separated from others by a distance large compared to l_c . At saddle points of the disorder potential lying at energies close to $E - E_n$, such that the distance between two contour lines becomes of order l_c , it breaks down. However, at these points the tunneling between different contour lines can be described by local 2×2 scattering matrices $S_j(E) = \{t_{ml}^j(E)\}$, relating the coefficients of incoming and outgoing currents by

$$\begin{pmatrix} \psi_m \\ \psi_n \end{pmatrix} = \begin{pmatrix} t_{mk}^j(E) & t_{ml}^j(E) \\ t_{nk}^j(E) & t_{nl}^j(E) \end{pmatrix} \begin{pmatrix} \psi_k \\ \psi_l \end{pmatrix}, \quad (10)$$

at all saddle points. For a given potential the scattering coefficients for the saddle points can be determined as functions of the energy E by semi-classical methods, as has been shown and explicitly worked out by Fertig [20]. Further, knowing the matrices $S(E)$, the scattering conditions (10) form a closed system of equations for the coefficients ψ_l from which eigenenergies E_n and eigenstate coefficients ψ_l can be determined [20].

Now, identifying the saddle points with nodes and the approximated contour states (9) with links, one arrives at a properly defined network. Finite isolated QH-Systems correspond to finite closed networks, systems coupled to external leads are described by open networks. Network states $\Psi = \{\psi_l\}$ determine wave functions of the real system via the expressions (9). Moreover, the scattering condition (10) fulfilled by eigenstates of the QH-system is just the stationarity condition of the network; thus eigenenergies E_n and -states Ψ_n are determined by

$$U(E_n)\Psi_n = \Psi_n, \quad (11)$$

corresponding to Eq. (4.7) in Ref. [20]. Here the network operator $U(E)$ is energy dependent, since the coefficients are functions of energy.

The Chalker-Coddington model is basically identical to such a network, but exhibits some simplifications: It's nodes and links form a regular square lattice, in contrast to saddle points and contour lines of a real smooth disorder potential, which may give a more irregular network. Further, for all nodes the transmission amplitudes for the scattering into the left outgoing links is set to a constant value T_+ , and for the scattering into the right link to $T_- = 1 - T_+$. The scattering phases $\phi_{lm} = \arg t_{lm}$ are random variables, homogeneously distributed over $[0, 2\pi]$, as in the case of the network model for a real disorder potential. The scattering amplitude T_+ acts as model parameter.

With these simplifications the network can be viewed as one corresponding to a QH-system with an egg-carton-like disorder potential. The basic length a of this potential is assumed to be large compared to l_c . Also it should exhibit small deviations from regularity, such that the flux penetrating the plaquettes fluctuates strongly on scales of Φ_0 , leading to random scattering phases ϕ_{lm} . According to this picture we parameterize the transmission amplitude by $T_{\pm} = (1 + \exp(\pm E/E_t))^{-1}$, where E denotes the electron energy (minus the cyclotron energy $\hbar\omega_c(n + 1/2)$) and E_t a characteristic tunneling energy of the saddle points. Thus, the Chalker-Coddington network is build up by nodes with scattering matrices

$$S_j = \begin{pmatrix} e^{i\varphi_j(\varepsilon)} & 0 \\ 0 & e^{i\varphi'_j(\varepsilon)} \end{pmatrix} \begin{pmatrix} t_+(\varepsilon) & t_-(\varepsilon) \\ -t_-(\varepsilon) & t_+(\varepsilon) \end{pmatrix}, \quad (12)$$

where $t_{\pm}(\varepsilon) = (1 + e^{\pm\varepsilon})^{-1/2}$ and $\varepsilon = E/E_t$. These nodes are arranged on a regular square lattice with orientation as shown in Fig. 2(b). For fixed ε the scattering phases $\varphi_j(\varepsilon), \varphi'_j(\varepsilon)$ are considered to be random numbers homogeneously distributed over $[0, 2\pi]$; except for this they are not further specified. As it has been shown by the originators, the network exhibits delocalized states only at a singular critical point determined by $|t_-| = |t_+|$, i.e. at $\varepsilon_c = 0$. For $\varepsilon \neq 0$ the eigenstates have a finite localization length ξ , diverging with a universal exponent $\nu \approx 2.3$ when ε approaches $\varepsilon_c = 0$, $\xi \propto |\varepsilon|^{-\nu}$ [4].

The ε -dependent network operator of the model is given by the coefficients of the scattering matrix (12) via Eq. (3). Then the network dynamics are

$$\Psi(t) = U^t(\varepsilon)\Psi(0), \quad t = 0, \pm 1, \pm 2, \dots \quad (13)$$

ε -dependent quasi-energies $\omega_n(\varepsilon)$ and eigenstates $\Phi_n(\varepsilon)$ are defined by

$$U(\varepsilon)\Phi_n(\varepsilon) = e^{i\omega_n(\varepsilon)}\Phi_n(\varepsilon), \quad (14)$$

the local density of network states is

$$\rho_\varepsilon(l, \omega) = \sum_n |\phi_{n,l}(\varepsilon)|^2 \delta(\omega - \omega_n(\varepsilon)). \quad (15)$$

Quenched disorder is represented by the random phases ϕ_j . Thus the disorder average of a quantity A is given by the integral over all random-phase configurations, $[A] \equiv \int_0^{2\pi} \prod_j \frac{d\phi_j}{2\pi} A\{\varphi_m\}$. As usual, in numerical calculations this ensemble average is approximated by the average over a finite set of disorder configurations $\{\varphi_m\}$. In case of local observables A_l the statistics are often improved by taking also a system average $[A]_S = N^{-1} \sum_{n=1}^N A_n$.

A generalized version of this model is obtained, when also the transmission amplitudes become random variables, e.g. by $t_\pm^j = (1 + \exp(\varepsilon - \mu_j))^{-1/2}$, where $\mu_j \in [-W/2, W/2]$ is random and independent for each node j . This type of disorder corresponds to fluctuating saddle point energies of the random potential, which brings in aspects of classical percolation [7,9,26].

The 3D model we will investigate is very similar to that of Chalker and Dohmen [10]. It consists of a stack of the 2D Chalker-Coddington networks we just have considered, now coupled into the vertical direction by interlayer links as shown in Fig. 4. However, the local scattering

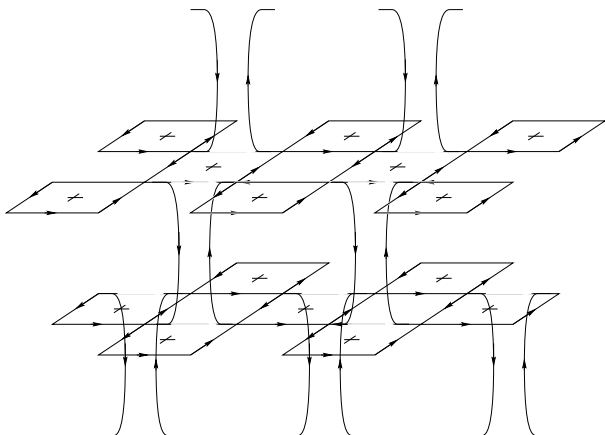


FIG. 4. Structure of the 3D network model.

matrices are defined as in the 2D network; so here the scattering amplitudes are also determined by the energy-parameter ε and the disorder is represented by random scattering phases. Due to the inter-layer coupling, the singular delocalized point at $E = 0$ of the 2D network becomes an extended metallic band ranging from $-E_c$ to E_c , $E_c > 0$. Outside this band the states are localized [10].

IV. PHASE COHERENT DIFFUSION IN DISORDERED SYSTEMS

The standard method to determine numerically a quantum particle's time evolution is first to calculate all

eigenvalues E_n and eigenvectors ϕ_n of the Hamiltonian. After that, the state at any time t of a particle initially in state $\psi(0)$ can be calculated simply by

$$\psi(t) = \sum_n e^{-iE_n t} \langle \phi_n, \psi(0) \rangle. \quad (16)$$

In this procedure, the diagonalization of the Hamiltonian takes the main part of the numerical effort and limits the application of this method to rather small system sizes*.

The dynamical network model offers a far better way to simulate quantum mechanical time evolution. Using the network dynamics Eq.(5), one can evolve any arbitrary state $\Psi(0)$ in discrete time steps by iterative multiplication of $\Psi(0)$ with the network operator U ,

$$\Psi(t) = U^t \Psi(0) = U \Psi(t-1), \quad t = 0, 1, 2, \dots, \quad (17)$$

Since multiplication of vectors by matrices is one of the simplest tasks computers can perform (particularly when most of the matrix entries vanish, as in our case) the dynamics are very suitable for numerical applications. In fact, by this the simulation of the quantum mechanical time evolution becomes as easy as the simulation of a classical system with discrete dynamics.

Let us consider numerical calculations for the 2D and 3D networks described in the last section. In both cases we investigate the spreading of network states initially confined to a few links in the center of a squared (cubic) network of volume L^d . The diffusion of such states is described by the disorder averaged ($[\dots]$) probability density

$$p(r, t) = [\psi(r, t)^2]. \quad (18)$$

($\psi(r, t)$ understood as the link amplitude $\psi_l(t)$ at link l closest to coordinate r .) We will determine this density for states at energies in the metallic, the insulating and in the transition regime. The latter regime is especially interesting, since at this energy interference effects start to destroy the diffusion [1].

Before the setups are explained in detail and results are presented, let us briefly summarize some results concerning quantum diffusion in disordered systems. For the transition point, these results are gained mainly from scaling theory [28,29].

At energies deep in the metallic regime the density $p(r, t)$ is given by the Gaussian density,

*For example, the Hamiltonian for a 3D system of $L \times L \times L = 50 \times 50 \times 50$ lattice points possesses 50^3 energy levels and as many eigenvectors with 50^3 complex entries each. This yields approximately $(50^3)^2 \approx 1.6 \times 10^{10}$ complex numbers, equivalent to at least about 100 Giga Byte, which to calculate or to back up is a hard job, also for today's computers.

$$p(r, t) = \frac{1}{(4\pi Dt)^{d/2}} e^{-r^2/4Dt}, \quad (19)$$

where D is the diffusion constant (ordinary diffusion). Accordingly, the q th moment of the density grows like

$$M_q(t) \equiv \int d^d r r^q p(r, t) \propto t^{hq} \quad (20)$$

with exponent $h = 1/2$.

In the vicinity of the transition point, scaling theory predicts an algebraic decay of the density at short distances $r \ll (t/\rho_c)^{1/d}$

$$p(r, t) \propto t^{-D_2/d} r^{D_2-d}, \quad (21)$$

where D_2 is the correlation dimension of critical eigenstates and ρ_c the density of states at the transition point [27–29]. At large distances, $r \gg (t/\rho_c)^{1/d}$, the decrease of the density is still exponential. From this follows that at the critical point the q th moment scales like [29]

$$M_q(t) \propto t^{q/d}. \quad (22)$$

Therefore, in $d > 2$ dimensions, the exponent h shrinks down from $1/2$ in the metallic regime to the lower critical value $1/d$ when the transition point is approached, indicating the transition to the localized regime, where diffusion ceases.

In the localized regime, the wave-packet spreads out until its size has become of the order of the localization length ξ . Up to this point the density $p(r, t)$ evolves in the same way as at the critical point. At larger times, $t \gg \rho_c \xi^d$, the density equilibrates in a volume ξ^d , centered around the starting point.

Now, let us consider the outcomes of our computer simulations. We begin with the diffusion on the Chalker-Coddington network at critical energy $E_c = 0$. The initial state $\Psi(0)$ is located on four links labeled by 0,1,2,3 in the center of a squared closed network with periodic boundary conditions,

$$\Psi(0) = \frac{1}{2}(\mathbf{e}_0 + \mathbf{e}_1 + \mathbf{e}_2 + \mathbf{e}_3). \quad (23)$$

This state is subjected to the time evolution Eq. (5), whereby $E = E_c$. Figure 5 visualizes the diffusion of a particle on a 40×40 node network and also demonstrates the numerical precision of the simulations. The

FIG. 5. A state evolving backwards after it has moved 350 time steps forward. The initial state is reconstructed to a high accuracy (last picture of the lower row).

first picture in the upper row shows the density $|\Psi(r, t)|^2$ after 350 time steps. The initial state $\Psi(0)$ has been almost equilibrated over the whole lattice. In order to

test that this equilibration is by no means influenced or even caused by accumulating numerical errors, we applied successively the adjoint operator $U^+ = U^{-1}$ on the final state $\Psi(350)$. Doing this, the state evolves back (see Fig. 5) and returns after another 350 steps to the initial state with high accuracy, $|\Psi' - \Psi| < 10^{-14}$.[†]

Fig. 6 shows the q th moment $M_q(t)$ to the power of $2/q$ for $q=2,4$ and 6 at critical energy $E_c = 0$ and in the strong localized regime at energy $E = 3E_t$. The data for

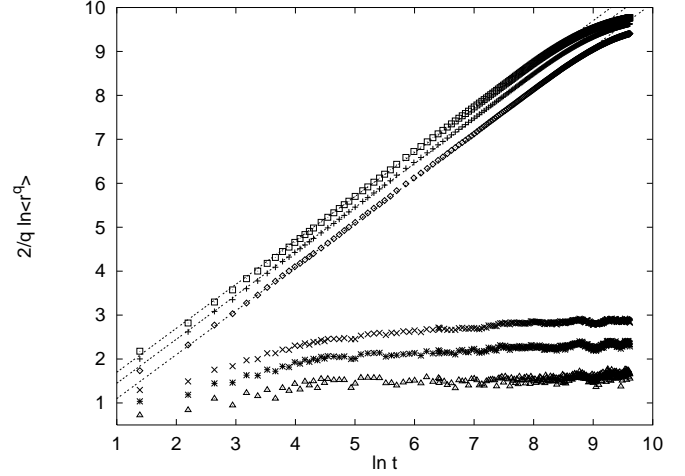


FIG. 6. The 2nd (\diamond), 4th ($+$) and 6th (\square) moment (to the power of $2/2$, $2/4$ and $2/6$, respectively) of spreading wave-packets at the transition point at energy $E = E_c = 0$ and in the strong localized regime, $E = 3E_t$ (where \triangle , $*$, \times correspond to the 2nd, 4th and 6th moment). The dashed lines have slope 1.

E_c are gained from 5 networks of 300×300 nodes with periodic boundary condition. Since the moments are obtained by integration over the entire system, their fluctuations with respect to different disorder configurations are quite small; the average of 5 configurations yields moments proportional to $M_q(t) \propto t^{qh}$, with an exponent h very close to $1/d = 1/2$ (see Fig. 6). At times greater than the diffusion time of order $\ln t_L = \ln(L/2)^2 \approx 9$ the increase goes down, since then the extension of the wave-packet has reached the system size L . Away from the critical point, the moments saturate quickly at cer-

[†]The stability of the quantum mechanical time evolution against numerical errors seems to be quite astonishing, since it is in sharp contrast to the numerical instability of the classical counterpart. Because of the chaotic dynamics, in the latter the numerical uncertainty in position and impulse makes the trajectory of a classical particle completely indefinite after a few time steps. However, the dynamical stability of quantum-chaotic systems is well-known and has been first observed by Shepelyansky [30].

tain values, reflecting the absence of diffusion at length scales greater than the localization length.

Next, we consider the probability of the particle to return to the initial volume formed by the links $l = 0, 1, 2, 3$,

$$p(t) = \sum_{l=0}^3 |\psi_l|^2. \quad (24)$$

Since this return probability fluctuates strongly with respect to disorder, it is necessary to average over many configurations. The curve plotted in Fig. 7 results from 400 different critical networks of 100×100 nodes each. The return probability decays with a power law, $p(t) \propto t^x$, with exponent $x = 0.76 \pm 0.01$.

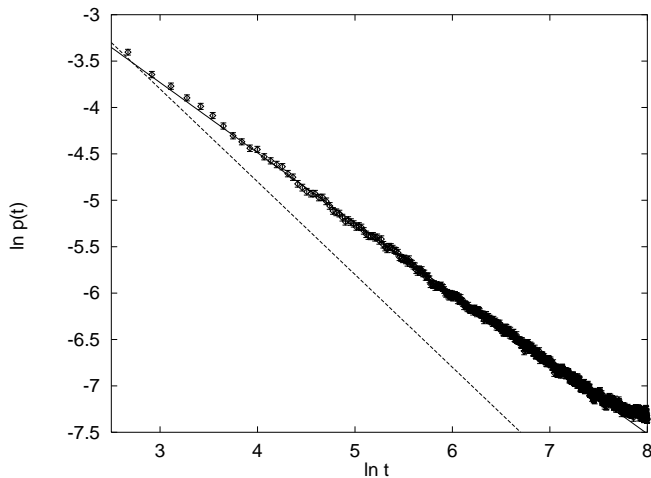


FIG. 7. The averaged return probability $p(t)$ taken from 400 networks of 100×100 nodes each. The data fits to a straight line with slope $x = 0.76 \pm 0.01$. The dashed straight line with slope -1 corresponds to normal diffusion.

In accordance to Eq. (21), this exponent fits well to the correlation dimension for critical states, which is exactly twice that, $D_2/2 = 0.75 \pm 0.025$ (see Sec. VI). The straight line with slope -1 corresponds to the decay of the return probability one would expect for classical diffusion, governed by Eq. (19).

Finally, we discuss the density $p(r, t)$ for fixed times t as a function of r . In order to reduce the numerical effort, we average $p(r, t)$ over a ring of radius r around the origin:

$$\bar{p}_t(r) = \frac{1}{2\pi} \int p(|r|, \varphi, t) d\varphi. \quad (25)$$

Taking for granted that the disorder averaged density $p(|r|, \varphi, t)$ is radially symmetric, the new density $\bar{p}_t(r)$ exhibits the same scaling behavior as $p(r, t)$. However, due to the integration over the ring $\bar{p}_t(r)$ fluctuates much less than $p(r, t)$, which considerably reduces the number

of configurations necessary for a satisfyingly small statistical error. Because of Eq. (21), the curves $\bar{p}_t(r)$ for different times t should coincide for small radii r after rescaling them by

$$\bar{p}_t(r) \longrightarrow t^{D_2/2} \bar{p}_t(r). \quad (26)$$

The averaged density $\bar{p}_t(r)$ of five critical systems of 300×300 nodes and times t ranging from $t = 1500$ up to 15000 steps shows that this is indeed the case (Fig. 8). The algebraic decay of the density for small r changes

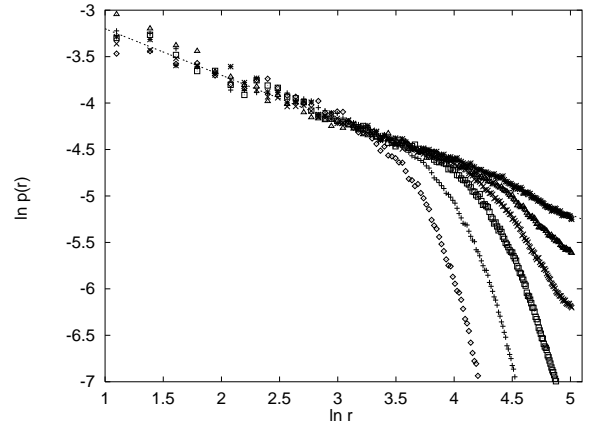


FIG. 8. The rescaled density $t^{D_2/2} \bar{p}_t(r, t)$ for times $t = 1500$ (\diamond) up to 15000 (*). The straight lines corresponds to $r^{D_2-d} \approx r^{-0.5}$.

to an exponential decay at radii larger than a crossover length, which increases with time t . The data plotted in Fig. 8 for small r fits to r^{D_2-d} , with $d - D_2 = 0.5$, as predicted by Eq. (21).

For the 3D model we carried out analogous simulations. We first determined the moments $M_q(t)$ for states initially restricted to a plaquette in the center of a cubic network of $L^3 = 50^3$ nodes. In Fig. 9 the moments $M_q(t)^{2/q}$ are plotted for $q = 2, 4, 6$ at energies $E = 1.5, 3.4$ and 6, measured in units of the tunnel energy E_t . The average of 5 disorder configurations has been taken. At energy $E = 1.5$ the moments scale with an exponent $h = 1/2$, indicating pure metallic diffusion according to Eq. (19), for $E = 6$ the moments converge to finite values small compared to L^q , which shows clearly the absence of diffusion, i.e. localization. For energies $E = 3.4 \pm 0.1$ we found an anomalous reduced exponent h very close to $1/3$. Consequently, energy $E = 1.5$ must be in the metallic and $E = 6$ in the strongly localized regime. The transition energy we determined to be $E_c = 3.4 \pm 0.1$, since at energies 3.3 and 3.5 significant deviations from the critical scaling $M_q(t) \propto t^{q/3}$ are already visible.

The return probability $p(t) \propto t^{-x}$ shown in Fig. 10 results from 200 systems of size $L^3 = 50^3$ at critical energy $E = 3.4$. From these data we obtained $x = 0.43 \pm 0.04$

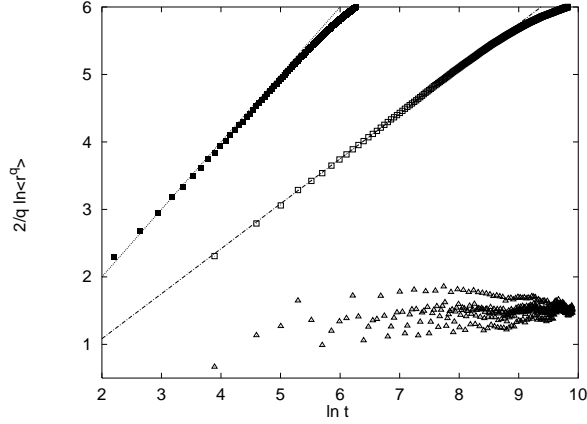


FIG. 9. The second moment $M_2(t)$ at energies $E = 1.5$ (filled \square), 3.4 (\square) and 6 (\triangle), corresponding to the metallic, transition and isolating regime of the 3D network model, respectively.

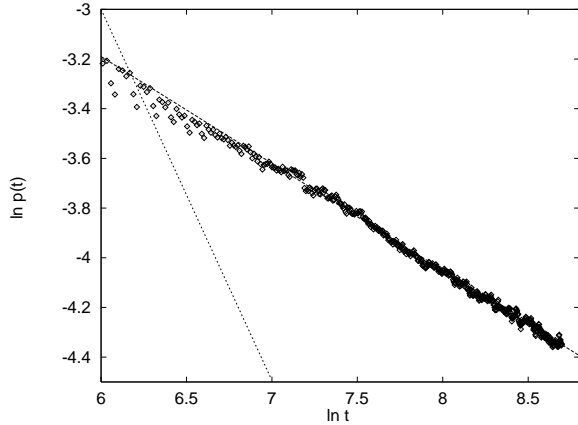


FIG. 10. The critical return probability decays proportional $\propto t^{-D_2/3}$, $D_2/3 = 0.43 \pm 0.04$. Data obtained from 200 systems of 50^3 nodes each. The dotted line with slope $-3/2$ corresponds to normal diffusion.

and thus $D_2 = 3x = 1.3 \pm 0.12$ according to Eq. (21). For the 3d Anderson transition this correlation dimension has not yet been determined very precisely. The values obtained in previous publications are $D_2 = 1.7 \pm 0.3$ [31], $D_2 \approx 1.45 - 1.8$ [32] and $D_2 = 1.7 \pm 0.2$ [29]. An analytical calculation using an epsilon expansion yields $D_2 = 2 - \epsilon = 2 - (3 - 2) = 1$ [33]. It should be noted that the network model corresponds to a system with a magnetic field while in Ref. [31,32,29] time reversal systems in the absence of magnetic fields were considered.

Finally, Fig. 11 shows the density profile $\bar{p}(r, t)$ at time $t = 20000$ of states initially located in the center of the network in the metallic, critical and localized regime. At this time, metallic states at $E = 1$ have been completely equilibrated over the entire system, seen by the constant density $\bar{p}(r, t)$, whereas the density of states at $E = 6$

in the localized regime shows a strong, exponential decay. Both densities do not evolve further in time. At

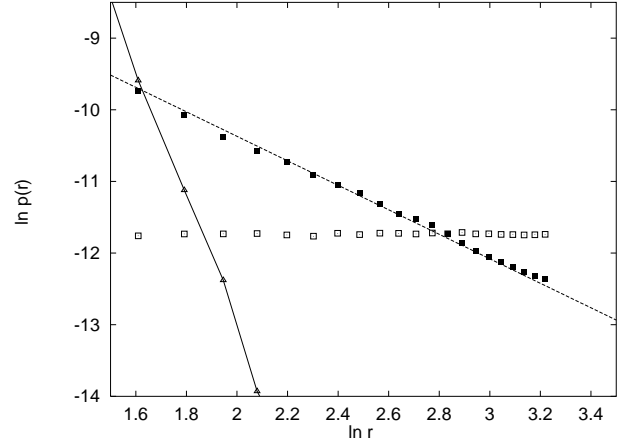


FIG. 11. The density $\bar{p}(r, t)$ at time $t = 20000$ of states initially located in the center of a 3D network of 50^3 nodes. The curves correspond to energies $E = 1E_t$ (metallic, \square), $E_c = 3.4E_t$ (critical, filled \square) and $E = 6E_t$ (localized regime, \triangle).

the transition point, just at time $t = 20000$ the bulk of the spreading wave-packets cover the whole lattice. Therefore, the corresponding density decays algebraically $\propto r^{-y}$ according to Eq. (21) with exponent y close to $\eta = 3 - D_2 = 1.7 \pm 0.1$.

To summarize the outcome of the simulations, both the 2D and 3D dynamical network models show precisely the expected diffusive behavior. The metallic regime of the 3D model shows normal diffusion with a Gaussian density $p(r, t)$. At the critical point in both systems the simulations fit very well to the anomalous diffusion predicted by scaling theory. It is also quite remarkable that the simple, locally defined dynamics (5) lead immediately to the well-known but highly non-trivial Anderson-localization, caused by long ranged destructive interferences.

Since dynamical network models correctly describe the dynamics of disordered systems in the metallic, localized and even in the transition regime, their generating operator U must necessarily contain relevant information on the spectral properties in the corresponding regimes. Certainly, this information is encoded in the quasi-spectrum $\{\omega_n\}$ of $U(E)$, on which we will focus now.

V. SPECTRAL STATISTICS

We start with the investigation of the *local* spectral density $\rho_0(\omega)$ of the two models under consideration. After that we turn over to the statistics of quasi-energy-level distribution in the Chalker-Coddington network. As be-

fore, particular attention is paid to the metal-insulator transition point.

A. Local Spectral Density

The local spectral density can be calculated efficiently by iteration in nearly the same way as before the return probability $p(t)$. Instead of the return probability Eq. (24) one has to determine the complex amplitude $\psi(0, t) = \langle \mathbf{e}_0, U^t \mathbf{e}_0 \rangle$, i.e. the propagator $G_{00}(t)$. In principle, Fourier-transforming the latter immediately yields the spectral density $\rho_0(\omega) = \sum_n |\Phi_n(0)|^2 \delta(\omega - \omega_n)$ because of

$$G_{00}(t) = \langle \mathbf{e}_0, U^t \mathbf{e}_0 \rangle = \sum_n e^{i\omega_n t} |\Phi_n(0)|^2 \quad (27)$$

$$= \int d\omega e^{i\omega t} \rho_0(\omega). \quad (28)$$

Thus, to obtain the local spectral density $\rho_0(\omega)$ we generate the sequence $G_{00}(t), t = 0, 1, \dots, T$ successively by applying U on the state \mathbf{e}_0 . Before doing the numerical Fourier transformation, we softened the sharp edges of the time-window from 0 to T by multiplication with $1/2 - 1/2 \cos(2\pi t/T)$ (the so called Hamming window), in order to reduce artifacts due to the finite time range. Additionally, to ensure numerical stability, we damped the Green function with the exponential $e^{-t/\tau}$, whereby the damping time τ fulfills $1 \ll \tau \ll T$. Then, performing a discrete Fourier transformation on this windowed and damped Green function and taking the real part of the result we get the quantity

$$\rho'_0(\omega) = \sum_n |\phi_n(0)|^2 \delta_\tau(\omega - \omega_n), \quad \omega_n = \frac{2\pi}{T} n, \quad (29)$$

where $\delta_\tau(\omega)$ is a peaked function with maximum value at $\omega = 0$ and width of order $1/\tau$. For sufficiently large times τ and $T \gg \tau$, this quantity converges to the wanted density $\rho_0(\omega)$.

By this method, the spectral densities plotted in Fig. 12 of a Chalker-Coddington network of 50×50 nodes have been calculated, whereby we chose $\tau = 2000$ and $T = 32768$. In the upper spectrum, at energy $E = 2E_t$, the density is almost concentrated at only a few energies, reflecting strong localization. The lower, critical spectrum at $E_c = 0$ fluctuates strongly and turns out to be scale invariant, as we will see in a moment.

The same method applied to the 3D network model considered above gave the three spectra shown in Fig. 13, corresponding to the localized, critical and delocalized regime. For the calculations we used systems of $50 \times 50 \times 50$ nodes, a maximum time $T = 32768$ and $\tau = 4000$. At energy $E = 6$ in the localized regime and at the transition point $E_c = 3.4$ the spectra are qualitatively similar to the corresponding ones of the 2D model, whereas at

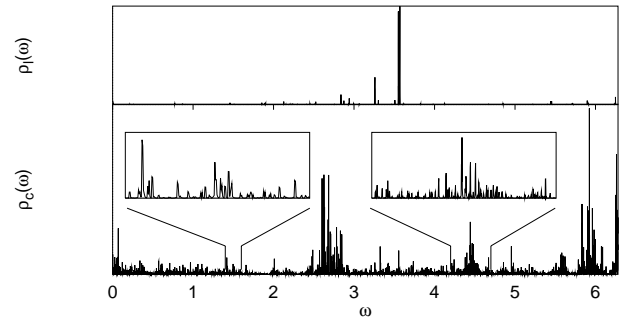


FIG. 12. Local spectral density $\rho_0(\omega)$ of the 2D Chalker-Coddington network of 50×50 nodes in the localized regime at $E = 2E_t$ (upper) and at the transition point (lower) at $E = E_c = 0$. The localized density is concentrated on few frequencies, indicating strong localization. The critical density is distributed over the entire band and appears to be scale invariant.

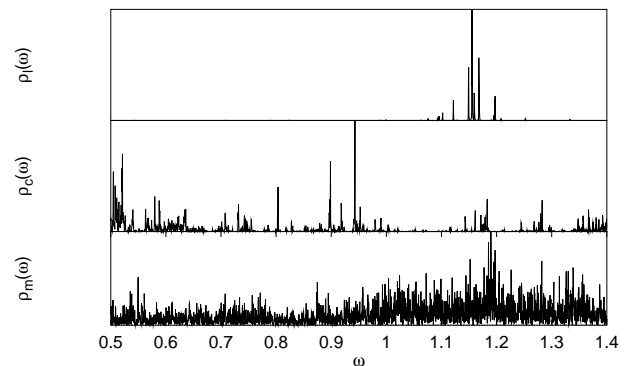


FIG. 13. Local spectral densities of a 3D network model of 50^3 nodes in the localized ($E = 6E_t$), critical ($E = 3.4$) and metallic ($E = 1$) regime.

energy $E = 1$, where states are delocalized, the spectrum is comparatively homogeneous.

The critical spectral densities deserve a closer look. Their scale invariance (or self-similarity) can be demonstrated by examining the scaling behavior of the quantity $m(\Omega) = \int_{\omega_0}^{\omega_0 + \Omega} \rho_0(\omega) d\omega$, which is the mass of the interval $[\omega_0, \omega_0 + \Omega]$ with respect to the density $\rho_0(\omega)$. Disorder averaged powers of it, $m_q(\Omega) = \langle m^q(\Omega) \rangle$, scale over a wide frequency (Ω) range with definite exponents, as can be seen by the linear dependence of $\ln m_q(\Omega)$ on $\ln \Omega$, plotted in Fig. 14. This power law scaling of $m^q(\Omega)$ proves the scale invariance of the density $\rho_0(\Omega)$. Unlike in the case of homogeneous densities, the scaling exponent depends nonlinearly on q , therefore the densities are called multifractals [34]. They can be characterized by generalized dimensions \tilde{D}_q describing the scaling of the $m_q(\Omega)$ by $m_q(\Omega) \propto \Omega^{d+(q-1)\tilde{D}_q}$, for, in principle, all real q . d denotes the dimension of the density's support, thus

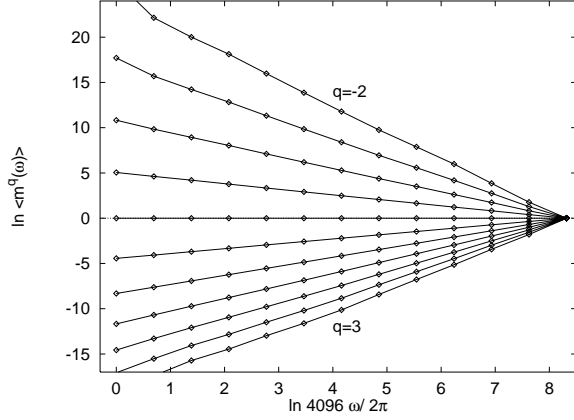


FIG. 14. Scaling behavior of q th powers of masses $m(\Omega) = \int_{\omega_0}^{\omega_0+\Omega} \rho_0(\omega) d\omega$ for box sizes Ω from $2\pi/4096$ up to 2π and powers q ranging from -2 to 3 in steps 0.5. The data result from the average over non overlapping intervals of 28 systems of 200×200 nodes each.

$d = 1$ for the spectral measure. [‡] Figure 15 shows the generalized dimensions of the critical spectral densities of both, the 2d and the 3d model. For the determination of the \tilde{D}_q we use 28 2d systems of 200×200 nodes and 5 3d systems of $50 \times 50 \times 50$ nodes, respectively. The

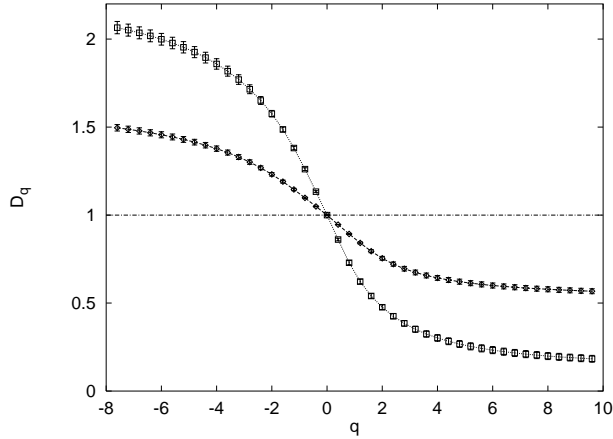


FIG. 15. Generalized dimensions of critical local spectral densities in the 2D (\diamond) and 3D (\square) network model.

values for some characteristic exponents, namely the information dimension \tilde{D}_1 , the correlation dimension D_2 , $D_{-\infty}$, D_{∞} , and the quantity $\tilde{\alpha}_0 = d - \partial \tilde{D}_q / \partial q (q = 0)$ are listed in Tab. I. The coincidence of the correlation

[‡] Equivalently, instead of the generalized dimension \tilde{D}_q often also exponents $\tau_q \equiv (q-1)\tilde{D}_q$ or the Legendre transformed $f(\alpha)$ of the function τ_q are used to describe a multifractal density [34].

Dim.	\tilde{D}_1	\tilde{D}_2	$\tilde{D}_{-\infty}$	\tilde{D}_{∞}	$\tilde{\alpha}_0$
2d	0.87 ± 0.01	0.75 ± 0.01	1.5 ± 0.2	0.6 ± 0.1	1.14 ± 0.01
3d	0.67 ± 0.02	0.48 ± 0.03	2.1 ± 0.1	0.2 ± 0.2	1.34 ± 0.2

TABLE I. Generalized dimensions and $\tilde{\alpha}_0$ of critical local spectral densities in the 2D and 3D network model.

dimension $\tilde{D}_2 = 0.75 \pm 0.02$ and 0.48 ± 0.03 respectively with the decay exponents of the return probability $p(t)$, $x = 0.76 \pm 0.01$ and 0.43 ± 0.04 is not by accident, but because $\rho_0(\omega)$ and $p(t) = |\psi_0(t)|^2$ are related via $\psi_0(t)$ by Fourier transformation, which implies that x equals \tilde{D}_2 [35].

B. Quasi-Energy Level Distribution in the Chalker-Coddington Network

By interpreting U as a time evolution operator, the eigenphases ω_l of the unimodular eigenvalues $e^{i\omega_l}$ of U must be considered as the analog to energy levels. In the following we will consider the distribution of these eigenphases or quasi-energy levels $\omega_l(\varepsilon)$ of the Chalker-Coddington network. We will determine the level spacing distribution function $P(s)$ and the level number variance $\Sigma_2(N)$. $P(s)ds$ gives the probability to find a quasi-energy level at distance sds of another level, whereby s is measured in units of the average level spacing Δ . $\Sigma_2(N) \equiv \langle (n - \langle n \rangle)^2 \rangle$ denotes the variance of the number of levels in an interval which contains on average $\langle n \rangle = N$ levels.

The investigated systems are closed networks with periodic boundaries of $L \times L = 50 \times 50$ nodes in the localized and critical regime at energies $E = 10$ and $E = E_c = 0$, respectively. The corresponding unitary network operators $U(E)$ are represented by $M = 2 \times 50 \times 50$ dimensional matrices. Diagonalizing such a matrix by standard numerical methods yields M complex eigenvalues $e^{i\omega_l(E)}$, homogeneously distributed on the unit circle. The corresponding quasi-energy levels $\omega_n(E)$ are homogeneously distributed in the interval $[0, 2\pi[$ with an averaged spacing $\Delta = 2\pi/M$. It is not necessary to perform special unfolding-procedures in order to compensate inhomogeneities in the distribution. For these quasi-level distributions $\omega_l(E)$ we determine $P(s)$ and $\Sigma_2(s)$.

Fig. 16 shows the level distribution function $P(s)$ for networks in the localized regime at energy $E = 10$ and at the transition point at $E = E_c = 0$. Since for $E = 10$ the networks states are strongly localized, their eigenvalues (quasi-energies) are uncorrelated, reflected by the Poisson distribution $P(s) = \exp(-s)$. Accordingly, the level number variance is given by $\Sigma_2(N) = N$ (Fig. 17).

At the transition point, eigenstates are extended giving rise to a strong level repulsion, as can be seen by the corresponding level distribution function, which resembles

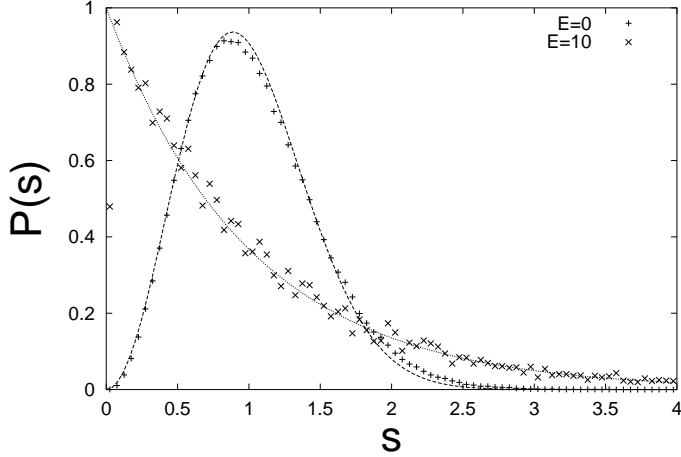


FIG. 16. The level distribution function $P(s)$ for quasi-levels of networks in the localized regime, $E = 10$ (\times), and at the transition point $E = E_c = 0$ ($+$). In the localized regime the distribution is clearly governed by Poisson statistics (solid curve), whereas it is close to the Wigner surmise for a unitary ensemble (dashed line) at the transition point.

the Wigner surmise for a unitary ensemble (Fig. 16). However, Fig 17 shows that the level number variance is

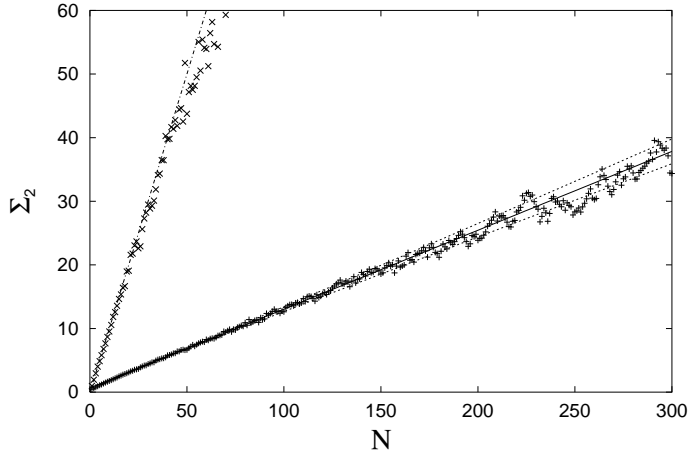


FIG. 17. Level number variance $\Sigma_2(N)$ for quasi-levels of networks in the localized regime, $E = 10$ (\times), and at the transition point, $E = 0$ ($+$).

still linear in N , $\Sigma_2(N) = (0.124 \pm 0.006) \times N$. This is in contrast to metallic behavior, where $\Sigma_2(N) \propto \ln(N)$, but resembles the localized phase where $\Sigma_2(N) = N$. The difference to the latter is only the reduced proportionality constant, the spectral compressibility, $\chi = 0.124 < 1$. This value of the spectral compressibility fits to the result of Chalker et al. [24], according to which $\chi = (2 - D_2)/2d$, D_2 being the correlation dimension of critical states in Quantum Hall systems [13]. The non-vanishing com-

pressibility is reflected by a longer tail in the level spacing distribution. As predicted by Altshuler et al. [25] the tail of $P(s)$ decreases as $\exp(-\kappa s)$, where $\kappa = 1/(2\chi) \approx 4$. In [23,14,15] this relation could be verified for the Anderson model and the Chalker-Coddington model, respectively. Since there is no real metallic phase in the QHE, we cannot give examples for metallic quasi-level distributions from the Chalker-Coddington network.

For the 3D network this is possible. Fig 18 shows that the levels spacing distribution in the localized and metallic regime at energies $E = 0$ and $E = 10$ agree well with Poisson statistics and the Wigner surmise for a unitary ensemble, respectively. (Data obtained from 40000 quasi-energy levels of $10 \times 10 \times 10$ nodes networks.) The

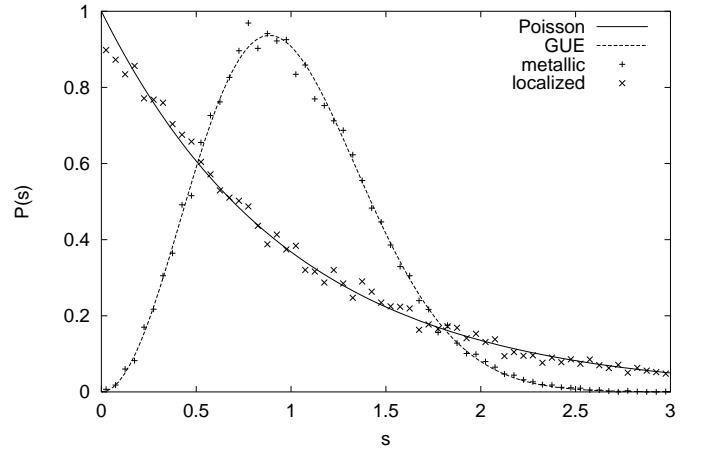


FIG. 18. Level distribution function $P(s)$ for quasi-levels of 3d networks in the localized ($E = 10$, \times) and metallic ($E = 0$, $+$) regime. The data fit well to Poisson statistics (solid curve) and to the Wigner surmise for a unitary ensemble (dashed line), respectively.

corresponding level number variances plotted in Fig. 19 indicates Poisson statistics in the localized regime and show the strongly suppressed variances for the metallic regime.

These two examples demonstrate that the distribution of network specific quasi-energy levels is equivalent to the distribution of real energy levels, as could be anticipated from the fact that network models correctly reproduce the dynamical properties of real physical systems.

Another argument supporting this equivalence relies on the symmetries and homogeneity of the flow of the quasi-energy levels $\omega_l(E)$ as a function of the real energy E . It can be found in [13].

VI. EIGENSTATES OF THE NETWORK

Correlations between eigenvalues of random matrices come along with certain correlations in the amplitudes

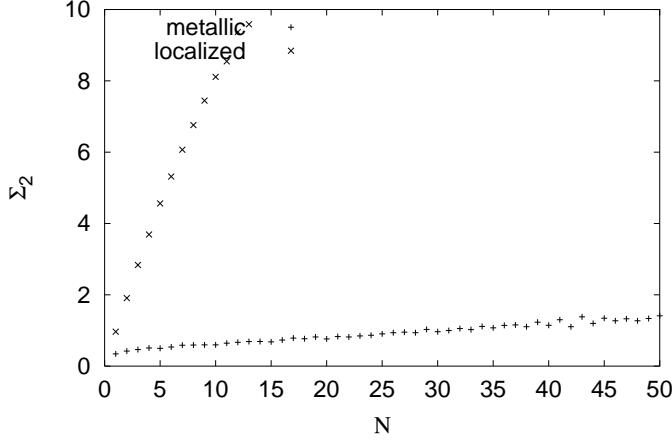


FIG. 19. Level number variance $\Sigma_2(N)$ for quasi-levels of 3d networks in the localized (\times) and the metallic ($+$) regime.

of eigenstates, which will be the subject of this section. As before, we investigate correlations of the Chalker-Coddington network, whereby we confine ourself to the critical region. Our findings for the network model will be compared to results obtained within other, conventional models, describing Quantum Hall systems with short range disorder by a tight-binding Hamiltonian [36] and by a so-called random Landau model [37].

Network eigenstates Ψ_n at energy E are solutions of the eigenvalue problem

$$U(E)\Psi_n = e^{i\omega_n}\Psi_n. \quad (30)$$

Notice that the energy E is fixed and only the quasi-energy ω_n varies. A particular eigenstate Ψ_n with link amplitudes $\{\psi_l\}_{l=1,\dots,N}$ refers to a spatial wave function $\Psi(r)$ via the link locations r_l by identifying $\Psi(r_l) \equiv \psi_l$. This rather vague definition is satisfactory as long as the considered length scales are large compared to microscopic scales.

Fig. 20 shows the square-amplitude $\rho(r) = |\Psi(r)|^2$ of a typical eigenstate obtained in the Chalker-Coddington network at critical energy $E = E_c = 0$. Like the local spectral density (see Sec. V A), the eigenstate exhibits a self-similar, multifractal structure, generic for the localization-delocalization transition point. Similar

FIG. 20. Squared amplitude of a Critical wave functions in a Chalker-Coddington network of 256x256 saddle points. Darker areas denote lower square amplitude.

as for the local spectral density, the scale invariance of the eigenfunctions can be demonstrated by investigating the scaling behavior of the quantity

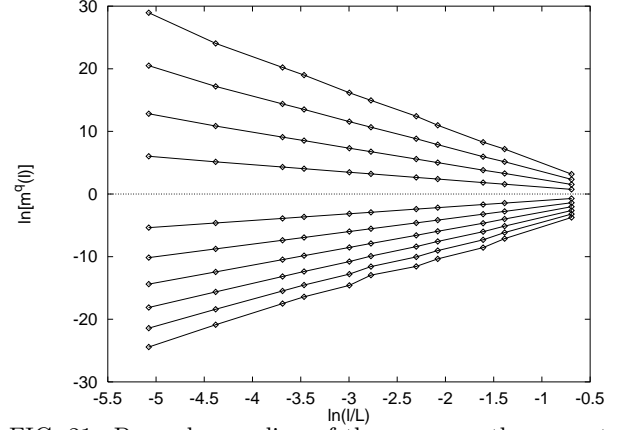


FIG. 21. Power-law scaling of the average q th-moment of box masses $m_q(l)$ for q -values from -2.0 to 3.0.

$$m(l) = \int_{l^2} d^2r \rho(r_0 + r), \quad (31)$$

which is the mass of a square of linear dimension l with respect to the density $\rho(r)$. The disorder averaged q th-moments of it, $m_q(l) = \langle m^q(l) \rangle$, obeys power law behavior over a wide range of box-sizes l , as can be seen in the double logarithmic plot in Fig. 21. The data were taken from the wave function in Fig. 20. The generalized dimensions D_q of the critical density $\rho(r)$, defined by $m_q(l) \propto l^{d+(q-1)D_q}$ ($d = 2$), are plotted in Fig. 22. For the determination of these exponents we used networks with sizes varying from 80×80 up to 512×512 and of two different kinds of boundary conditions, full-periodic and semi-periodic ones. To calculate eigenfunctions we applied the method of inverse iteration and, to treat larger systems, the Lanczos algorithm. Significant deviations in the multifractal exponents for networks of different sizes and boundary condition were not found. The results are also independent on the used numerical method. Table II

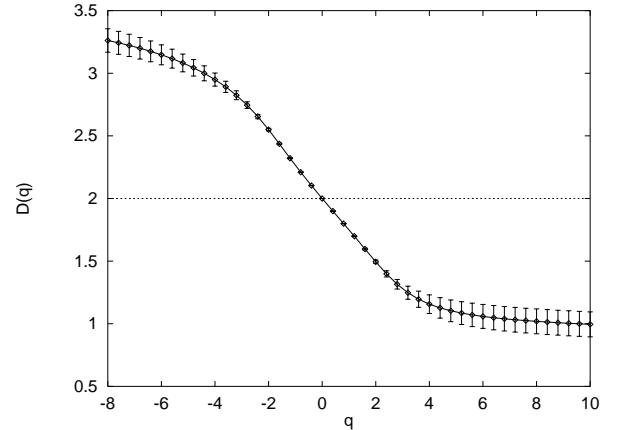


FIG. 22. The function $D(q)$ averaged over 12 wave functions.

lists some characteristic exponents and gives a comparison to the results obtained in the two models mentioned above. The exponent α_0 is defined as the derivative of D_q with respect to q at $q = 0$. The values for the multifractal exponents of these models match within the errors. The corresponding exponents of the critical local density

Model	D_1	D_2	$D_{-\infty}$	D_{∞}	α_0
N	1.75 ± 0.01	1.50 ± 0.01	3.4 ± 0.2	1.1 ± 0.1	2.26 ± 0.01
TB	-	1.62 ± 0.02	3.7 ± 0.2	1.0 ± 0.1	2.29 ± 0.02
RL	-	1.5 ± 0.1	3.7 ± 0.02	0.95 ± 0.2	2.3 ± 0.07
D/\bar{D}	2.01 ± 0.02	2.00 ± 0.02	2.3 ± 0.4	1.8 ± 0.4	1.98 ± 0.02

TABLE II. Comparison of characteristic multifractal exponents for different models: network (N), tight-binding (TB) and the Random Landau (RL) model. The last row gives the ratio of corresponding exponents for critical eigenstates and critical local spectral density.

of states (with tilde) appear to be half of those of the critical states. This simple proportionality, $D_q = d\bar{D}_q$, where $d = 2$ is the spatial dimension, is a consequence of dynamical scaling introducing a single energy dependent length scale $L_\omega \propto \omega^{-1/d}$ [12].

VII. TWO-POINT-CONDUCTIVITIES

Finally, we come to an example of an open network. We will study a Chalker-Coddington network coupled to external reservoirs via ohmic contacts, in order to demonstrate how the network model can be used for the determination of conductivities. For simplicity we assume the coupling to the reservoirs is given by two ideal point contacts: two links, a and b , of a closed network in a distance r are cut and connected to external reservoirs of chemical potential μ_a, μ_b , respectively see Fig. 23. This means that, firstly, the incoming channels a' and b' are occupied up to the chemical potentials μ_a, μ_b , secondly, the currents in the outgoing channels a and b are ideally absorbed by the reservoirs. The goal is to calculate the (dimensionless) conductance g of this configuration obeying the equation $\delta I = e/h g \delta \mu$, where $\delta \mu = \mu_a - \mu_b$ and δI the net current flowing through the network from reservoir a to b . Here the entire network can be viewed as a single scattering center – with quite complex internal structure – connecting the two incoming channels (a', b') to the outgoing ones (a, b). So, according to the Landauer-Büttiker formula, the conductance g is in this case the corresponding scattering amplitude $|t_{ab}|^2$ from a' to b , which to determine is our task. To do this, consider the following situation: let the incoming channel a' be feed by a unit current with amplitude 1 and set the amplitude in the other one, b' , to 0. The current will distribute over the network obeying (i) the boundary condition $\psi_{a'} = 1, \psi_{b'} = 0$ at the external incoming links a', b'

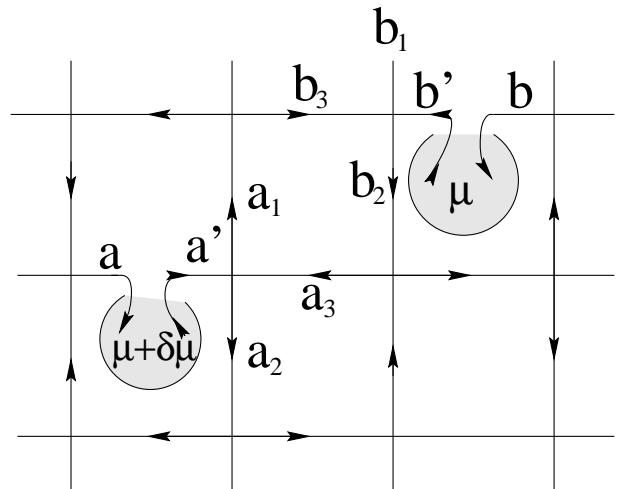


FIG. 23. Chalker-Coddington network coupled to external reservoirs by two point contacts.

and (ii) the local scattering conditions $\psi_l = \sum_m t_{lm} \psi_m$ at internal links l (including a and b). Then, ψ_b , the amplitude in outgoing channel b , equals exactly t_{ab} , the coefficient we are looking for. It is straightforward to show that conditions (i) and (ii) are equivalent to the vector equation

$$U(\Psi - \psi_a \mathbf{e}_a + \mathbf{e}_a - \psi_b \mathbf{e}_b) = \Psi, \quad (32)$$

where all quantities refer to the *closed* network. The term $-\psi_a \mathbf{e}_a$ belongs to the current reflected back into reservoir a , $+\mathbf{e}_a$ corresponds to current fed into channel a' , and $-\psi_b \mathbf{e}_b$ is due to current out-flowing through channel b' . With projection operators $\bar{P}_l = 1 - P_l = 1 - |\mathbf{e}_l\rangle\langle\mathbf{e}_l|$ Eq. (32) reduces to

$$(1 - U \bar{P}_a \bar{P}_b) \Psi = U \mathbf{e}_a,$$

and we obtain finally,

$$\begin{aligned} t_{ab} &\equiv \psi_b \equiv \langle \mathbf{e}_b, \Psi \rangle \\ &= \langle \mathbf{e}_b, (1 - U \bar{P}_a \bar{P}_b)^{-1} U \mathbf{e}_a \rangle. \end{aligned}$$

By this, the problem of finding the two-point conductance is reduced to a standard problem of linear algebra, which we solved by numerical LU-decomposition. In the following we will present data obtained by this method for critical Chalker-Coddington networks.

At criticality the conductances are expected to show a power law behavior with respect to the distance $r \ll L$ between the contacts, while their distribution will be very broad for any r . Furthermore, as was pointed out by Zirnbauer [8], there should not be a dependence of the conductance on the system size. As we will see, such a picture is consistent with our data. We have determined conductances for systems of size $L = 40, 60, 100$ and distances between links varying from $r = 1$ to $r = L/2$. For

every distance we determined up to 1300 conductances (depending on the system size).

The broadness of the distribution suggests to determine the moments $[g^q]$, the geometric mean $g_t = \exp[\ln g]$ and the log-variance $[(\ln g/g_t)^2]$. In Fig. 24 we show $[\ln g]$ plotted against $\ln r$ for three different system sizes $L = 40, 60, 100$. There is no visible L dependence, as expected, and the typical value scales in a power law fashion with respect to r .

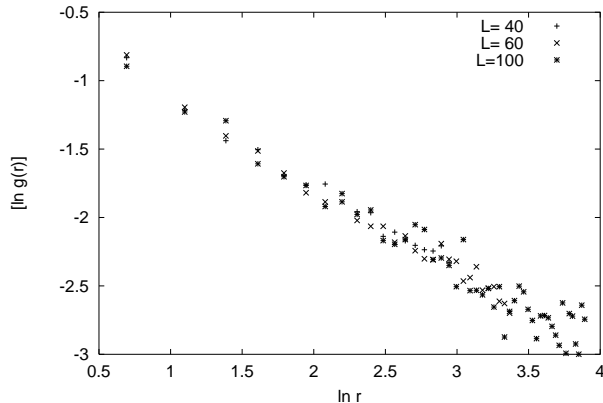


FIG. 24. The logarithm of the typical conductance plotted against $\ln r$ for three different system sizes.

We find similar behavior for the moments $[g^q]$, whose behavior can be described in the following way:

$$[g^q]_L \propto r^{-X(q)}, \quad (33)$$

where $X(q)$ is called the multifractal spectrum of the conductance. The numerical data for $X(q)$ for system sizes 40, 60 and 100 is depicted in Fig. 25. Within the

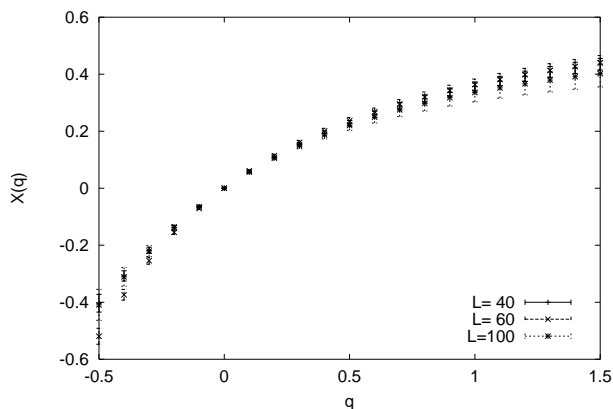


FIG. 25. The function $X(q)$ for three different system sizes.

error bars, the non-linear curves for different system sizes match, indicating universal multifractality. For further

information on the distribution $P(g)$ of the point-contact conductances see ref. [38].

VIII. SUMMARY

We extended the Chalker-Coddington model and a 3D generalization of it by a simple, discrete time evolution and studied dynamical and spectral aspects of the resulting dynamical network models. Despite of the simplicity of the dynamics, the models correctly show the universal aspects of normal and critical diffusion as well as of Anderson localization in temporal evolution of network wave functions. In case of closed networks, the analogue of eigenfunctions and eigenenergies exist in form of eigenvectors and quasi-energies (=eigenphases) of an unitary network operator. We investigated spatial and spectral correlation of eigenstates and quasi-energy spectra and found qualitative and quantitative agreement with theoretical predictions and other numerical work within conventional models. Furthermore, we used an open network for the calculation of two-point conductances.

Definitions and methods with regard to the network dynamics are not specific to the two models investigated in particular. Therefore, they should be as well applicable to any other model formulated as a network in terms of local scatterers and connecting link-channels.

Disregarding physical and mathematical subtleties, the analogies of a physical system described by a Hamiltonian H with it's corresponding network model represented by an unitary operator U can be summarized as in Tab. III. Notice that there are still significant differences:

$e^{-iH\tau}$	U
$\Psi(t) = e^{-iHt}\Psi(0)$	$\Psi(k\tau) = U^k\Psi(0)$
$H\psi_n = \varepsilon_n\psi_n$	$U\Psi_n = e^{i\omega_n}\Psi_n$
$\dots \varepsilon_{n-1}, \varepsilon_n, \varepsilon_{n+1}, \dots$	$\dots \omega_{n-1}, \omega_n, \omega_{n+1}, \dots$

TABLE III. Relation between Hamiltonian and network operator (schematic).

first of all, the dimensions of H and U do not match. The dimension of U equals the number of links, which generally is much smaller than the dimension of H , since each link-channel itself contains a large number of (quasi-) asymptotic states. In some sense, changing from H to U corresponds to reducing the original system by non-interesting degrees of freedom. In case of the models investigated here, these degrees of freedom are the link states: the network wave function Ψ no longer contains any information about their structure (e.g. wave number). Obviously, this dimensional reduction constitutes the main advantage of the network model, especially in numerical applications. The price to be paid for that is a loss of accuracy. Processes and correlations corresponding to length and energy scales of the out-projected in-

ternal degrees of freedom can no longer be reproduced. In particular this means that the statistical equivalence of energy and quasi-energy spectrum holds only in the vicinity of a certain energy E_0 to which $U = U(E_0)$ refers. Similarly, the network time evolution can only be related to the time evolution of real wave packets composed of eigenstates with energies close to E_0 .

ACKNOWLEDGMENTS

Fruitful discussions with János Hajdu, Martin Janssen and Bodo Huckestein are gratefully acknowledged. This work was performed within the research program of the Sonderforschungsbereich 341 of the Deutsche Forschungsgemeinschaft. M.M. thanks the Deutsche Forschungsgemeinschaft, R.K. the Minerva foundation (Munich, Germany) and the Weizmann Institute of Science (Israel) for support.

-
- ¹ Current address: Department of Condensed Matter Physics, Weizmann Institute of Science, 76100 Rehovot, Israel.
- ² Current address: Department of Physics, Toho University, Miyama 2-2-1, Funabashi, Chiba 274-8510, Japan.
- [1] P. W. Anderson, Phys. Rev. **109**, 1492 (1958).
[2] P. W. Anderson, D. J. Thouless, E. Abrahams, D. S. Fisher, Phys. Rev. B **22**, 3519 (1980).
[3] B. Shapiro, Phys. Rev. Lett. **48**, 823 (1982).
[4] J. T. Chalker, P. D. Coddington, J. Phys. C **21**, 2665 (1988).
[5] C. Flesia, R. Johnston, H. Kunz, Europhys. Lett. **3**, 497 (1987); Y. Avishai, Y. Hatsugai, M. Kohmoto, Phys. Rev. B **47**, 9561 (1993) A. W. W. Ludwig, M. P. A. Fisher, R. Shankar; G. Grinstein, Phys. Rev. B **50**, 7526 (1994); C.-M. Ho, J. T. Chalker, Phys. Rev. B **54**, 12 (1996); A. G. Galstyan, M. E. Raikh, Phys. Rev. Lett. **56**, 1422 (1997); D. P. Arovas, M. Janssen, B. Shapiro, Phys. Rev. B **56**, 4751 (1997); V. Kagalovsky, B. Horovitz and Y. Avishai, Phys. Rev. B **55**, 12 (1997); A. Hansen, E.H. Hauge, J. Hove and F.A. Maaø, Annual Reviews of Computational Physics **V**, 201 (1997); P. Freche, M. Janssen and R. Merkt, Phys. Rev. Lett. **82**, 149 (1999).
[6] I. Edrei, M. Kaveh, B. Shapiro, Phys. Rev. Lett. **62**, 2120 (1989).
[7] D.-H. Lee, Z. Wang, S. Kivelson, Phys. Rev. Lett. **70**, 4130 (1993);
[8] M.R. Zirnbauer, Ann. Physik **3**, 518 (1994).
[9] R. Klesse, M. Metzler, Europhys. Lett., **32**, 229 (1995).
[10] J. T. Chalker, A. Dohmen, Phys. Rev. Lett. **74**, 4496 (1996).
[11] T. Kottos, Uzy Smilansky, Phys. Rev. Lett. **79**, 4794 (1997).
[12] B. Huckestein, R. Klesse, Phys. Rev. B **55**, R7303 (1997).
[13] R. Klesse, M. Metzler, Phys. Rev. Lett. **79**, 721 (1997).
[14] M. Metzler and I. Varga, J. Phys. Soc. Jpn. **67**, 1856 (1998).
[15] M. Metzler, to be published in J. Phys. Soc. Jpn. (cond-mat/9809340).
[16] B. Huckestein, R. Klesse, Phil. Mag. B **77**, 1181 (1998); R. Klesse, Ph.D. Thesis, Universität zu Köln (AWOS-Verlag, Erfurt, 1996).
[17] M. Tsukada, J. Phys. Soc. Jpn. **41**, 1466 (1976).
[18] R. E. Prange, R. Joynt, Phys. Rev. B **25**, 2943 (1982).
[19] S. A. Trugman, Phys. Rev. B **27**, 7539 (1983).
[20] H.A. Fertig, Phys. Rev. B **38**, 996 (1988).
[21] S. V. Iordansky, Solid State Commun. **43**, 1 (1982).
[22] R. Prange, S. Girvin, *The Quantum Hall Effect*, 2nd ed. (Springer 1990); M. Janssen, O. Viehweger, U. Fastenrath and J. Hajdu, *Introduction to the Theory of the Integer Quantum Hall Effect*, edited by J. Hajdu (VCH, Weinheim, New York, Basel, Cambridge, Tokyo, 1994); B. Huckestein, Rev. Mod. Phys., **67** (1995).
[23] M. Batsch and L. Schweitzer, in *High Magnetic Fields in the Physics of Semiconductors II: Proceedings of the International Conference, Würzburg 1996*, edited by G. Landwehr and W. Ossau (World Scientific Publishers Co., Singapore, 1997), pp. 47–50.
[24] J. T. Chalker, I. V. Lerner, and R. S. Smith, Phys. Rev. Lett. **77**, 554 (1996); J. Math. Phys. **37**, 5061 (1996).
[25] B. L. Altshuler, I. Kh. Zharekeshev, S. A. Kotochigova and B. Shklovskii, JETP **67**, 625 (1988).
[26] M. Metzler, to be published in J. Phys. Soc. Jpn. (cond-mat/9809285)
[27] E. Abrahams, P. W. Anderson, D. C. Licciardello, V. Ramakrishnan, Phys. Rev. Lett. **42**, 673 (1994).
[28] J.T. Chalker and G.J. Daniell, Phys. Rev. Lett. **61**, 593 (1988).
[29] T. Brandes, B. Huckestein, L. Schweitzer, Ann. Physik **5**, 633 (1996).
[30] D. L. Shepelyansky, Physica D **8**, 208 (1983).
[31] C.M. Soukoulis and E.N. Economou, Phys. Rev. Lett. **52**, 565 (1984).
[32] M. Schreiber, Phys. Rev. B **51**, 663 (1995).
[33] F. Wegner, Z. Phys. B **25**, 327 (1976) and Z. Phys. B **35**, 207 (1979).
[34] M. Janssen, Int J. Mod. Phys. B **8**, 943 (1994).
[35] R. Ketzmerick, G. Petschel, T. Geisel, Phys. Rev. Lett. **69**, 695 (1992).
[36] B. Huckestein, B. Kramer, and L. Schweitzer, Surf. Sci. **263**, 125 (1992).
[37] W. Pook and M. Janssen, Z. Phys. B **82**, 295 (1991).
[38] M. Janssen, M. Metzler and M.R. Zirnbauer, to be published.